

# Interaction of nanoparticles with substrates: effects on the dipolar behaviour of the particles

F. Moreno, B. García-Cámara, J. M. Saiz and F. González

*Grupo de Óptica, Departamento de Física Aplicada, Universidad de Cantabria,  
Avd. de los Castros s/n 39005 Santander, SPAIN*

**Abstract:** In this work, we present a numerical analysis of the surface electric field of a metallic nanoparticle (either 2D or 3D) interacting with a flat substrate underneath. The influence of the distance to the substrate, particle size, the surrounding media and the substrate optical properties is analyzed as a function of the incident wavelength. We show that these are crucial factors that change the field distribution associated to the dipolar behavior of the particle. A useful parameter for illustrating the changes in the angular distribution is  $\theta_{max}$ , the angle at which the maximum of the surface electric field is located.

©2008 Optical Society of America

**OCIS codes:** (160.4236) Nanomaterials; (240.6680) Surface plasmons; (290.5850) Scattering, particles.

---

## References and Links

1. M. Kreuzer, R. Quidant, J. P. Salvador, M. P. Marco, and G. Badenes, "Colloidal-based localized surface plasmon biosensor for the quantitative determination of stanozolol," *Anal. Bioanal. Chem.* DOI 10.1007/s00216-008-2022-z.
2. A. Agrawal, R. Deo, G.D. Wang, M. D. Wang, and S. Nie, "Nanometer-scale mapping and single-molecule detection with color-coded nanoparticle probes," *PNAS* **105**, 3298-3303 (2008).
3. Y. C. Cao, R. Jin, and C. A. Mirkin, "Nanoparticles with Raman Spectroscopic Fingerprints for DNA and RNA Detection," *Science* **297**, 1536-1540 (2002).
4. R. Jensen, J. Shermard, and S. Emory, "Single Nanoparticle Based Optical pH Probe," *Appl. Spectrosc.* **61**, 832-838 (2007).
5. N. Engheta, "Circuits with Light at Nanoscales: Optical Nanocircuits Inspired by Metamaterials," *Science* **317**, 1698-1702 (2007).
6. T. Kalkbrenner, U. Håkanson, and V. Sandoghdar, "Tomographic Plasmon Spectroscopy of a Single Gold Nanoparticle," *Nanolett.* **4**, 2309-2314 (2004).
7. K. G. Lee, H. W. Kihm, J. E. Kihm, W. J. Choi, H. Kim, C. Ropers, D. J. Park, Y. C. Yoon, S. B. Choi, D. H. Woo, J. Kim, B. Lee, Q. H. Park, C. Lienau, and S. Kim, "Vector field microscopic imaging of light," *Nature Phot.* **1**, 53-56 (2007).
8. F. Moreno, F. González, and J. M. Saiz, "Plasmon spectroscopy of metallic nanoparticles above flat dielectric substrates," *Opt. Lett.* **31**, 1902-1904 (2006).
9. J. Nelayah, M. Kociak, O. Stéphan, F. García de Abajo, M. Tencé, L. Henrard, D. Taverna, I. Pastoriza-Santos, L. M. Liz-Marzán, and C. Colliex, "Mapping surface plasmons on a single metallic nanoparticle," *Nature Phys.* **3**, 348-353 (2007).
10. J. R. Arias-González and M. Nieto-Vesperinas, "Radiation pressure over dielectric and metallic nanocylinders on surfaces: polarization dependence and plasmon resonant condition," *Opt. Lett.* **27**, 2149-2151 (2002).
11. J. L. de la Peña, F. González, J. M. Saiz, F. Moreno, and P. J. Valle, "Sizing particles on substrates. A general method for oblique incidence," *J. Appl. Phys.* **85**, 432 (1999).
12. J. L. de la Peña, J. M. Saiz, G. Videen, F. González, P. J. Valle, and F. Moreno, "Scattering from particles on substrates: visibility factor and polydispersity," *Opt. Lett.* **24**, 1451-1453 (1999).
13. G. Lévêque and O.J.F. Martin, "Optical interactions in a plasmonic particle couple to a metallic film," *Opt. Express* **14**, 9971-9981 (2006).
14. P. W. Barber and S.C. Hill, *Light Scattering by Particles: Computational Methods* (World Scientific, 1990).
15. P. B. Johnson and R. W. Christy, "Optical Constants of the Noble Metals," *Phys. Rev. B* **6**, 4370-4379 (1972).
16. L. Novotny and B. Hecht, *Principles of Nano-Optics* (Cambridge University Press, 2006).
17. C. Bohren and D. Huffman, *Absorption and Scattering of Light by Small Particles* (Wiley, 1983).
18. L. Sherry, S.-H. Chang, G. Schatz, and R. Van Duyne, "Localized Surface Plasmon Resonance Spectroscopy of Single Silver Nanocubes," *Nanolett.* **5**, 2034-2038 (2005).

19. X. Wei, X. Luo, X. Dong, and C. Du, "Localized surface Plasmon Nanolithography with Ultrahigh Resolution," *Opt. Express* **15**, 14177-14183 (2007).
  20. T. Kalr, M. Perner, S. Grosse, G. von Plessen, W. Spirkl, and J. Feldmann, "Surface-Plasmon Resonances in Single Metallic Nanoparticles," *Phys. Rev. Lett.* **80**, 4249-4252 (1998).
  21. H. Mertens, J. Verhoeven, A. Polman, and F.D. Tichelaar, "Infrared surface plasmons in two-dimensional silver nanoparticles arrays in silicon," *Appl. Phys. Lett.* **85**, 1317 (2004).
- 

## 1. Introduction

The physics of the electromagnetic interaction between light and metallic nanoparticles has been the focus of attention of many researchers during the last decade. The possibility of exciting local resonances with the consequent enhancement of the local electromagnetic field has opened new applications of metallic nanosized particles as biosensors, biomarkers, spectroscopic enhancers in SERS, etc. [1-4] Furthermore, as the resonant frequencies depend on the size, shape and optical properties of the particles as well as on those of the surrounding medium, it is possible to tune those resonances along the visible part of the spectrum and also in the near infrared, with applications in optical communications and computing [5].

In a great part of the aforementioned applications, nanoparticles are on or close to a substrate. This proximity makes the particles to interact with the surface underneath, modifying the properties of the resonant modes. Only recently some researchers have taken advantage of this effect by using metallic nanoparticles as probe nanoantennas for monitoring surfaces [6]. This has generated a new way of making optical microscopy of surfaces. The spectral shift and broadening of localized surface plasmon resonances produced, for instance, in gold nanoparticles, give information about the physical profile of the surface. In addition, microscopic imaging of the vector field close to a surface has been obtained by detecting the orientation of the dipole excitation induced in a gold nanoparticle [7]. Interestingly, both techniques have in common that near field information can be obtained through scattering measurements in the far field.

In spite of all the studies contributing to a better knowledge of this problem, there are some basic aspects that have gained importance with the irruption of technological applications in the nanoscopic domain. One of these aspects is the knowledge of the changes induced in the local field distribution as a function of the size, shape, aggregation, configuration of the surroundings, incident wavelength and also as a function of the proximity to the resonances of the constituents. In a previous paper [8], we analyzed numerically the interaction of a metallic nanoparticle with a dielectric substrate (a common experimental situation). When the particle is isolated or far from the substrate, the dipole character of the electric charge oscillation is clearly manifested. In this case, the distribution of the modulus of the electric field on the particle surface follows the typical "eight-shape" with its charge concentration maximum close to the equator of the particle. This constitutes the background of the microscope technique developed in [7]. As the particle approaches the surface, other charge oscillation modes appear and the modulus of the surface electric field shows deviations with respect to the unperturbed "eight-shape". This idea, the analysis of the field distribution, and in particular the location of the maximum around a nanoparticle, will be used in this work as a fast indicator of either the dominant interaction among the charges in the system or the oscillation mode transitions induced by the spectral evolution. In fact, in addition to a vast amount of numerical work, it has been recently shown that surface plasmons excited on isolated metallic nanoparticles can be experimentally mapped by electron energy-loss spectroscopic techniques [9]. We think that two important aspects are worth a detailed analysis under this perspective and constitute the objective of this research: First, the spectral correlation of the surface electric field distribution and the far-field radiation scattered by the system, either on or off the resonances, with special attention to the role played by the substrate underneath; and secondly, to show the usefulness of 2D computations as representative of 3D systems.

Many research papers on numerical computing of light scattering by random or deterministic surfaces (for instance, particles on or above substrates) have used 2D models for explaining interesting physical effects like the enhanced backscattering or the interaction of particles with substrates. The latter for application purposes like particle sizing, optical forces, near field optical microscopy, etc [10-12]. Other authors claim that they solve a 3D problem when their results show that it can be reduced to a 2D one, due to the kind of geometry they are dealing with [13]. For these cases, the physics involved in the different problems proposed has been well exposed and most of times the generalization to other more realistic 3D situations is quite straightforward. Such a reduction in the geometrical description has the obvious computing advantages derived from a proper discretization of the boundaries in the system (mainly, better accuracy, less noise, and a wider scope in the parameters, variable ranges and cases under analysis, because of the use of simpler codes and shorter computation times). However, for the kind of analysis proposed in this paper it is very convenient to know to what extent the behavior obtained in a 2D situation can be naturally applied to another 3D system.

In section 2 we will perform a comparison of the 2D and 3D geometries for the isolated particle case, confronting the results for the modulus of the electric field for a sphere and for a cylinder of the same radius and composition when light is incident normal to its axis. The conclusions of this part will serve to establish the bases for the following 2D analysis when a substrate is under the particle. The two most representative cases, those of dielectric and metallic substrates, will be studied in sections 3 and 4 respectively. In Section 5 the main conclusions of this work are summarized.

## 2. 2D and 3D geometries

We analyze the distribution of the electric field modulus on the surface of a cylinder (2D) and a sphere (3D) when illuminated under the same conditions. The calculations are performed by means of a conventional finite elements method to solve the electromagnetic wave equation and also through a slight modification of the programs contained in ref [14]. The scattering objects in our calculations are either an isolated infinitely long circular cylinder or an isolated sphere of the same radius  $R$ . In both cases we have considered that they are made of a noble metal (either silver or gold) [15]. These objects are illuminated by a plane wave whose direction of propagation, for the cylinder case, is perpendicular to its axis and whose polarization is linear, with the electric field oriented perpendicular to the axis of the cylinder. For an infinitely long circular cylinder, this is the component of the field that can excite to excite plasmon resonances. The surface electric field on the particle will be computed and represented as a function of the angular parameter  $\theta$ , within a meridian plane containing  $\vec{k}$  and  $\vec{E}_{inc}$  (see Fig. 1), with  $\theta=0^\circ$  corresponding to the bottom of the particle (or forward direction side) and  $\theta=180^\circ$  to the top (or backward direction side).

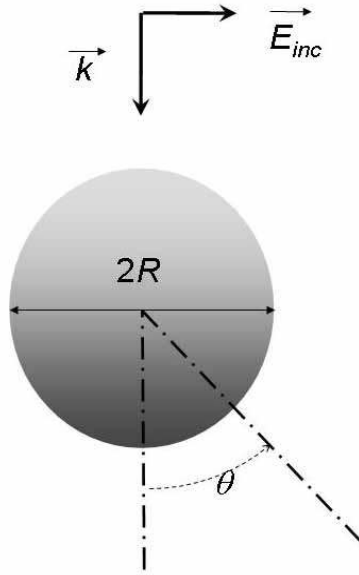


Fig. 1. Geometry of the system used in our calculations.

As a starting point, in Fig. 2 we show the angle ( $\theta_{max}$ ) at which the modulus of the surface electric field is maximum as a function of the particle radius  $R$ , for either an isolated silver sphere (full symbols) or an isolated silver cylinder (hollow symbols), and for three different values of the incident wavelength. The three selected values for  $\lambda$  are 360 nm, 420 nm and 480 nm (just to orientate, for a silver sphere these values would correspond to the resonance wavelengths for sizes  $R=20$ , 65 and 82 nm respectively) and the dependence of  $\theta_{max}$  with the wavelength is later analyzed in detail. In general, for an ideal dipole-like behavior ( $R \rightarrow 0$ ) and in the near field regime (roughly distances from the particle  $< \lambda/10$ ), the maximum of the modulus of the electric field will be symmetrically located at  $\theta=90^\circ$  and  $\theta=270^\circ$ , and the minima at  $\theta=0^\circ$  and  $\theta=180^\circ$  [16]. This is opposite to what happens in the far field where the distribution rotates  $90^\circ$  and the maxima and minima of the modulus of the scattered field would be located at  $\theta=0^\circ$ ,  $\theta=180^\circ$  and  $\theta=90^\circ$ ,  $\theta=270^\circ$  respectively. This corresponds to the typical eight-shaped distribution with its two lobes symmetric and perpendicular to the incident direction: An oscillating dipole does not radiate in the direction of oscillation. Parameter  $\theta_{max}$  seems to be quite sensitive to changes in the field distribution, and therefore to any effect that may produce a departure from the pure dipolar behavior.

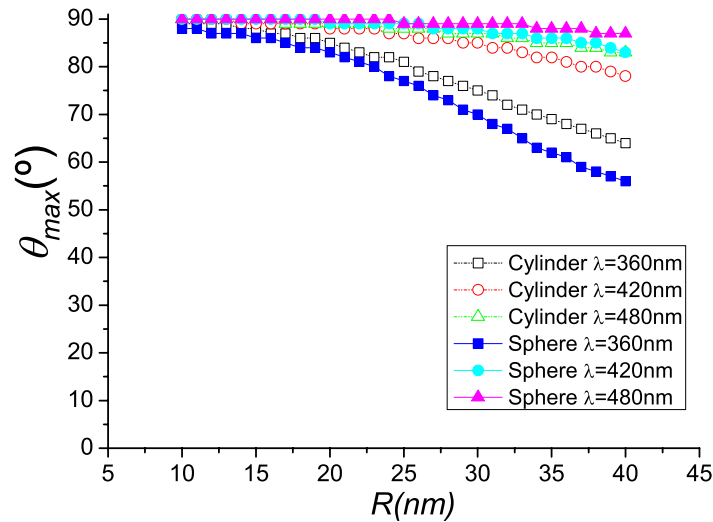


Fig. 2. Angular position of the maximum of the local electric field ( $\theta_{max}$ ) around an isolated silver sphere (full symbols) or an isolated silver cylinder (hollow symbols) as a function of the radius for several incident wavelengths.

In Fig. 2 such departure from  $90^\circ$  is clearly observed in a range of sizes from  $R=10$  to  $40$  nm, for which bulk optical properties can be considered. Obviously, small particles show a pronounced dipole-like behavior (all curves approach  $90^\circ$ ) and for increasing size the deviation is always monotonic, in most cases quite small, and tending to lower values of  $\theta$  (i.e. the local field “eight” lobes tend to the forward side of the particle). Values of  $\theta_{max}$  observed within the scattering plane show, in general, small differences between the sphere and the cylinder, and this supports the use of a 2D geometry to represent the perimetral distribution of the electric field, and even the far field, associated to 3D systems, provided that the scattering plane is orthogonal to the main (non-varying) direction.

In Fig. 3(a) we show the distribution of the modulus of the local electric field around an isolated silver cylinder for four different situations:  $R=25$  nm and  $\lambda=325$  nm (black squares);  $R=25$  nm and  $\lambda=348$  nm (a resonant wavelength, red circles);  $R=25$  nm and  $\lambda=370$  nm (green triangles) and  $R=50$  nm and  $\lambda=370$  nm (blue diamonds). For comparison, in Fig. 3(b) we show the distribution of the modulus of the local electric field around an isolated silver sphere for the same four different situations.

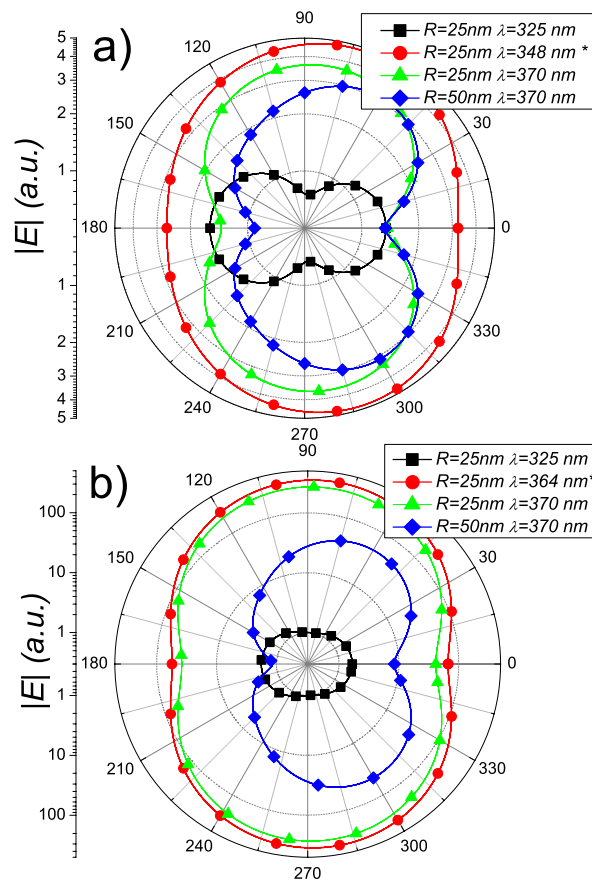


Fig. 3. Angular distribution of the local electric field at the surface of (a) an isolated silver cylinder and (b) an isolated silver sphere for three different incident wavelengths (at and around the plasmon resonance) and two different sizes. \* means that that wavelength is resonant for that geometry.

The distribution of the electric field around a small metallic cylinder out of resonance (green triangles) shows the typical eight-shaped dipolar distribution. If the particle size increases (blue diamonds), quadrupolar effects disturb the shape and the maxima of the electric field shift to the forward direction. Similar behavior occurs if the incident wavelength excites a resonance (red circles). The values of the modulus of the electric field increase as expected. In this case it is worthy to comment that for a cylinder of  $R=25\text{ nm}$  and for  $\lambda=348\text{ nm}$  there is a coincidence of the dipolar and quadrupolar resonances (see ref 8, Fig. 1). For this reason the typical “eight” shape is not clearly manifested. Furthermore there is a slight tendency to shift the maxima of the surface electric field to the forward direction. For lower wavelengths, the spatial distribution can be radically different from the dipolar behavior (black squares) due to effects that will be explained below. Now, the role played by  $\theta_{max}$  as an indicator of the distribution of the field shows its meaning. In this sense, it is illustrative to plot the evolution of  $\theta_{max}$  as a function of the wavelength.

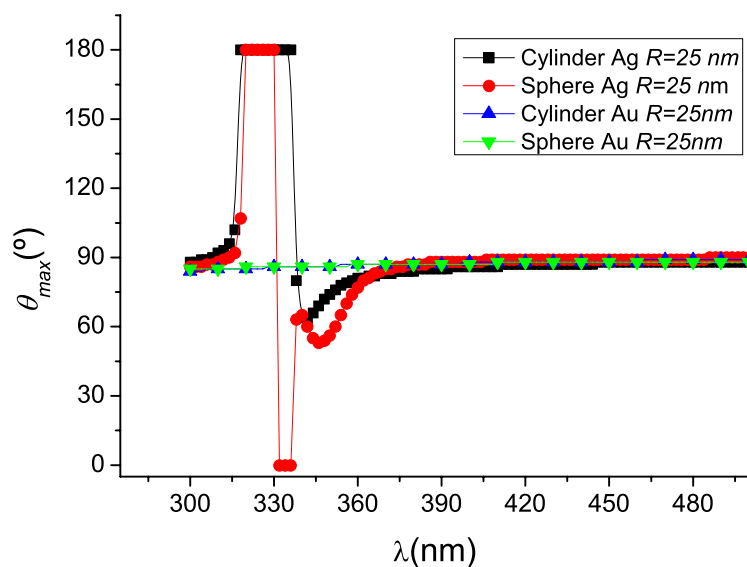


Fig. 4. Angular position of the maximum of the local electric field ( $\theta_{max}$ ) around an isolated cylinder made of silver (squares) or gold (up-triangles) and around an isolated sphere made of silver (circles) or gold (down-triangles) as a function of the incident wavelength and for the same size for all the cases.

The comparative curves shown in Fig. 4 correspond to a sphere and a cylinder made of silver or gold and of the same radius ( $R=25nm$ ). We see that for  $\lambda \geq 360 nm$ , the values of  $\theta_{max}$  saturate towards  $90^\circ$ , as corresponding to a purely dipolar behavior. This is a consequence of the optical constants (silver and gold are very good conductors) and the favorable ratio particle size/wavelength which makes the electrostatic approximation more accurate independently of the geometry and optical properties of the particle. However, for silver and  $\lambda < 360 nm$  the increasing ratio ( $R/\lambda$ ) combines with the particular evolution of the optical constants of silver, producing some features that are worth a comment. The dielectric constant for silver has an intricate dependence in the range  $\lambda \in [300, 360] nm$  (part of it due to interband transitions). Its real part changes its sign at around  $325 nm$ , and reaches the values of  $-1$  and  $-2$  at  $338 nm$  and  $355 nm$  respectively. The last two values correspond to the Frölich resonances [17] of an infinitely thin cylinder and a point-like sphere respectively. Around these values,  $\theta_{max}$  presents small departures from  $90^\circ$  that reach a minimum value at a wavelength that depend on the size of the particle and is located very close to the real resonances of the sphere and the cylinder (for  $R=25nm$ , the resonant wavelengths for the cylinder and sphere are respectively  $350$  and  $358 nm$ ). An abrupt change occurs when the modulus of the real part of the dielectric constant of the particle matches that of the surrounding medium. In our case this pseudo-matching is found for a  $\lambda \cong 338 nm$  where  $Re(\epsilon_{Ag}) \cong -1$ . This effect is independent of the particle size and only depends on the refractive index of the surrounding medium. This has been summarized graphically in Fig. 5 for silver cylinders. By comparing the curve with black squares and that with green triangles we observe that when the refractive index of the surrounding medium changes from  $1$  to  $1.5$ , the spectral position of the flip of  $\theta_{max}$  (from the top backward to the mid-forward part) shifts from  $338 nm$  to  $360 nm$  where  $|Re(\epsilon)| \cong 2.28$ , very close to  $(n')^2$ . Similar conclusions as those of Fig. 5 can be obtained for the spherical geometry. Only some quantitative differences around the minima of  $\theta_{max}$  will appear as has been outlined for Fig. 4.

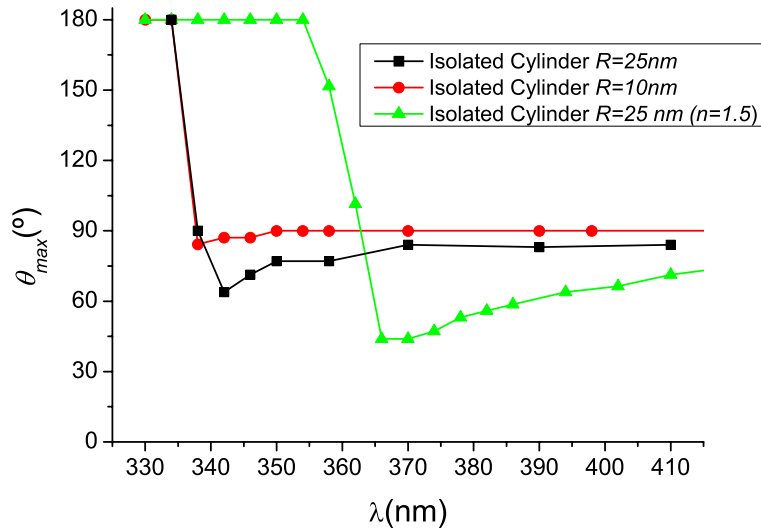


Fig. 5. Angular position of the maximum of the local electric field ( $\theta_{max}$ ) around an isolated cylinder for two different sizes and for a case in which the surrounding medium is denser ( $n=1.5$ ) than the air.

Interestingly, particles made of gold behave in a slightly different way than those made of silver in the range  $[300, 360]$  nm (see Fig. 4). The zero crossing of the real part of the dielectric constant occurs at a wavelength lower than  $300$  nm. In the range of wavelengths studied,  $Re(\epsilon_{Au})$  is always negative and never reaches the value  $-1$ . In this sense the dipole-like behavior is more clearly observed for gold than for silver in the whole range of wavelengths considered. As can be seen in Fig. 4, the values of  $\theta_{max}$  for gold stay very close to  $90^\circ$  for both geometries.

We can conclude that, under the conditions of our study, the distributions of the local electric field, the localization of its maxima and other effects (pseudo-matching, spectral localization of quadrupolar effects and resonances) present a qualitative parallelism between the cylindrical (2D) and spherical (3D) geometries. However, this correspondence can not be extended to a quantitative point of view. Therefore, and maintaining the last conditions (incident polarization, size and spectral range), we shall consider in what follows a 2D geometry, i.e. a metallic cylinder on or close to a flat substrate.

### 3. Particle above a dielectric substrate

In this section, local field calculations will be performed on a circular cylinder made of a noble metal of radius  $R$ , and located at a distance  $d$  above a semi-infinite surface (see Fig. 6). Taking into consideration the differences found for our 2D and 3D scattering systems, we may assume that the local electromagnetics involved in the scattering problem of a cylindrical object on a flat substrate is representative, to some extent, of that of an spherical particle on a flat substrate, for the same geometrical section and optical parameters, provided that both the illumination direction and the scattering plane are perpendicular to the main axis of the cylinder, and, more important, the polarization of the incident electric field is also normal to the cylinder axis. In other words, it should not surprise us that most of the results found for the cylinder geometry under these conditions could be extended to the spherical case. This does not apply necessarily to other profiles (in fact, irregular contour shapes induce very particular field distributions, as shown by a recent work [9]). The substrate will be considered made of either metal (next section) or dielectric, both very often used in many experimental situations

[18]. The system is illuminated by a linearly polarized wave whose propagation direction is perpendicular to both the cylinder axis and the substrate and whose electric field is perpendicular to the cylinder axis.

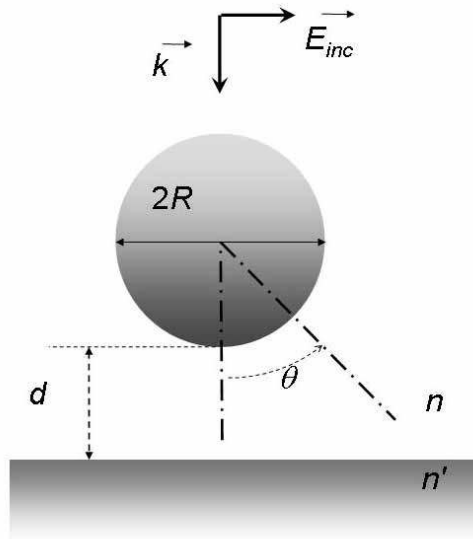


Fig. 6. Scheme of the geometry used for a system consisting of a metallic cylinder above a flat substrate.

The angle  $\theta$  at which the angular position of the modulus of the surface electric field is calculated is indicated in Fig. 6 following the same convention used for the isolated particle.

In Fig. 7 we show the evolution of  $\theta_{max}(\lambda)$  for a silver cylinder of radius  $R=25\text{ nm}$  in vacuum (optical constants from ref. [15]) above a dielectric substrate of  $n'=1.5$  for different values of  $d$  (1, 2, 5, 10 and 25 nm). The isolated case is also shown for comparison and the tendency towards this curve as  $d$  increases is clearly observed. It is interesting to correlate these plots with the plasmon spectra calculated in ref. [8] (see Figs. 1 and 3 of that work). The sudden decrease of  $\theta_{max}$  corresponds, as was mentioned in the previous section, to the pseudo-matching of the dielectric constant of the medium surrounding the cylinder ( $\epsilon=1$  in this case) with that of silver for a value of  $\lambda$  for which  $|\text{Re}(\epsilon_{Ag})|=1$ . After this flip of  $\theta_{max}$ , the maximum of the surface electric field tends to be located at the bottom part of the cylinder, i.e. the part facing the substrate. The spectral interval in which this effect happens gets longer as the particle approaches the substrate. The interaction with the substrate shifts to the red the wavelength at which the dipole-like behavior ( $\theta_{max} \rightarrow 90^\circ$ ) appears. This is in agreement with the red shift observed in ref [8] for the plasmon dipole resonance. Similar behaviour is observed when the particle size is increased.

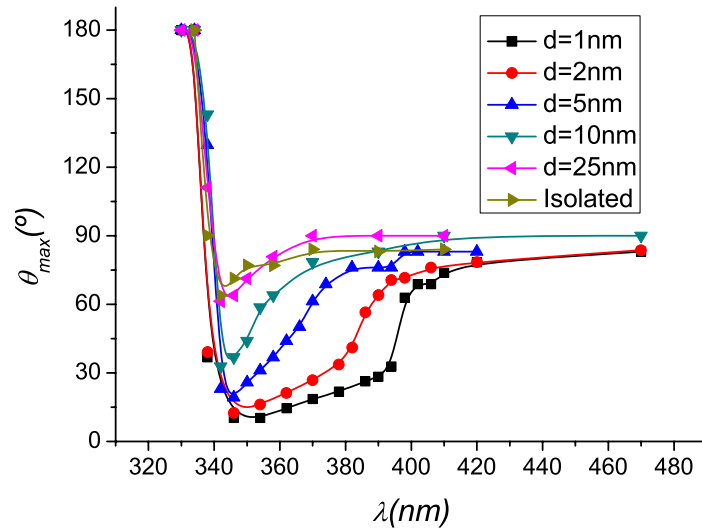


Fig. 7. Angular position of the maximum of the local electric field ( $\theta_{max}$ ) around a silver cylinder both isolated or above a flat substrate ( $n'=1.5$ ) as a function of the incident wavelength and for several values of the gap between the cylinder and the substrate.

In Fig. 8(a) we show, for comparison,  $\theta_{max}$  vs.  $\lambda$  for two sizes,  $R=25nm$  and  $R=10nm$  and the same distance  $d=1nm$ . The spectral range in which the maximum of the local electric field is facing the substrate gets narrower as the particle size decreases. A narrowing in that spectral range is also observed if the distance to the substrate is increased (see Fig. 8(b) for  $d=5nm$ ).

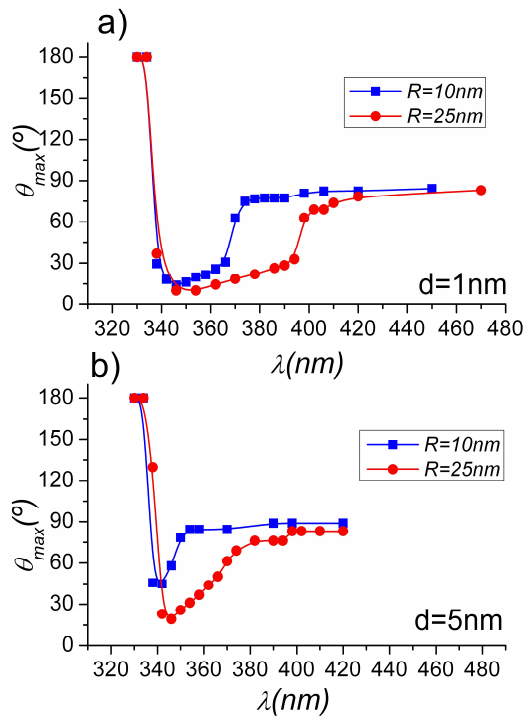


Fig. 8. Angular position of the maximum of the local electric field ( $\theta_{max}$ ) around a silver cylinder of two different sizes above a dielectric substrate ( $n'=1.5$ ) at a distance: (a) 1 nm and (b) 5 nm as a function of the incident wavelength.

As an example, the field distribution around the particle is shown in the polar plots of Fig. 9, for a silver particle of  $R=25\text{nm}$  at a distance  $d=1\text{nm}$  above a dielectric substrate ( $n'=1.5$ ) and for several incident wavelengths.

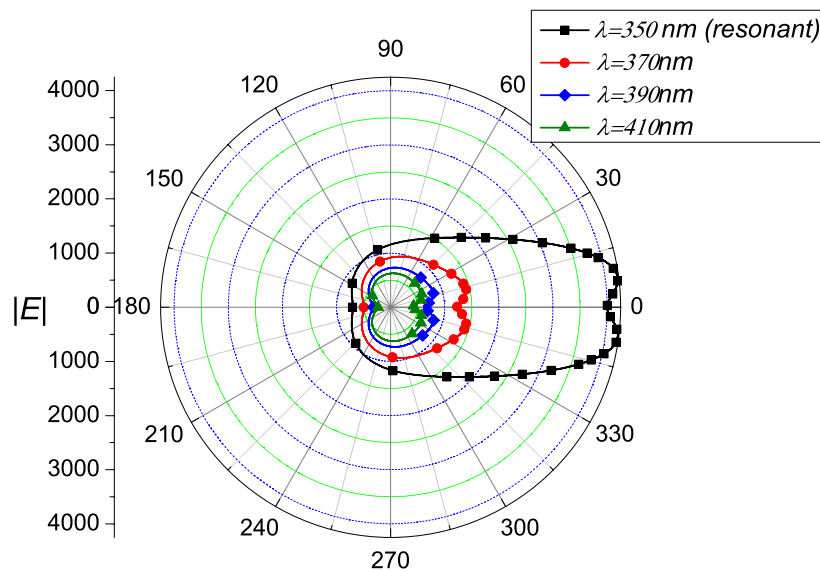


Fig. 9. Scattering diagram of a silver cylinder of  $R=25\text{ nm}$  and above a dielectric substrate ( $n'=1.5$ ) at a distance  $d=1\text{ nm}$  for several incident wavelengths.

As can be seen, the substrate produces a shift of the maximum towards the forward direction, and an overall change in the surface electric field distribution. In particular, for a resonant wavelength the intensity increases considerably and the distribution of the electric field shows an unusual shape with very high values on the side facing the substrate and an interesting double-point peak which can have possible applications on surface lithography at the nanoscale range [19].

The case of a cylinder immersed in a medium denser than the substrate is interesting because it corresponds to real practical experimental situations [20, 21]. As was mentioned in [8], this situation produces a blue-shift of the plasmon resonance due to the reinforcement of the electric charge oscillation in the particle. In other words, the sign of the reflection coefficient of the interface does not change when  $n > n'$  and the reflected field produces a constructive superposition. This situation is represented in Fig. 10 for which  $R=25\text{ nm}$ ,  $d=1\text{ nm}$ ,  $n'=1$  and  $n$  takes two different values:  $n=1.5$  (■) and  $n=1.3$  (●). The case  $n=1$ ,  $n'=1.5$  has been included for comparison (see broken line with triangles).

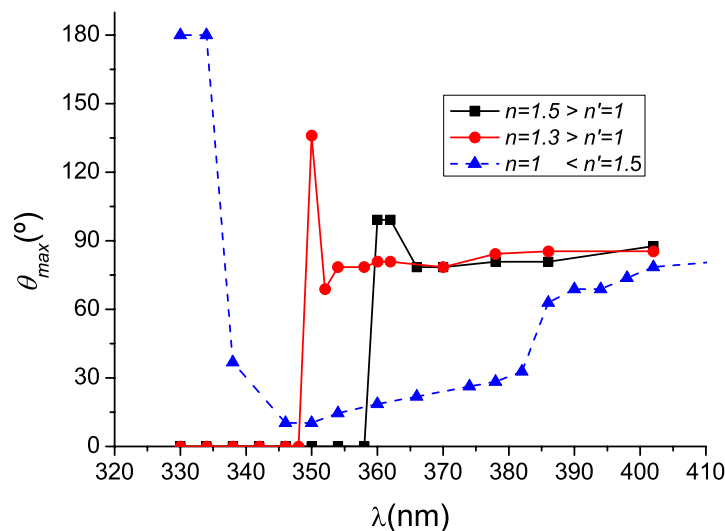


Fig. 10. Angular position of the maximum of the local electric field ( $\theta_{max}$ ) around a silver cylinder ( $R=25 \text{ nm}$ ) above a flat substrate at a distance  $d=1 \text{ nm}$  as a function of the incident wavelength and for different combinations of the refractive index of the surrounding medium and the substrate.

When  $n > n'$  the dipolar behavior ( $\theta_{max} \cong 90^\circ$ ) occurs at shorter wavelengths than for  $n < n'$ . Furthermore, this is always preceded by a transition region whose flip position corresponds to the wavelength where the pseudo-matching is produced (the dielectric constant of the particle surrounding medium matches that of  $|Re(\epsilon_{Ag})|$ ).

In order to complete this study, Fig. 11 shows some results corresponding to a cylinder made of gold. Triangles ( $\blacktriangle$ ) are for  $R=25 \text{ nm}$  and for the isolated case in vacuum. Squares ( $\blacksquare$ ) and circles ( $\bullet$ ) represent the evolution of  $\theta_{max}$  for cylinders of  $R=10 \text{ nm}$  and  $R=25 \text{ nm}$ , respectively, in vacuum and located  $1 \text{ nm}$  above a substrate of  $n'=1.5$ . The angle  $\theta_{max}$  does not show any special feature and it always keeps close to  $90^\circ$ , very different to what happens with silver. This behaviour is intimately related to the  $\lambda$ -dependence of the optical constant of gold [15]. However, if the surrounding medium is denser than the substrate, solid diamonds ( $\blacklozenge$ ) and magenta stars ( $\star$ ) in Fig. 11, there is a different behaviour of the surface electric field below and above the wavelength at which  $|Re(\epsilon_{Au})|$  matches the dielectric constant of the surrounding medium ( $\lambda=494 \text{ nm}$  for  $n=1.5$ ,  $n'=1$ , and  $\lambda=440 \text{ nm}$  for  $n=1.3$ ,  $n'=1$ , approximately).

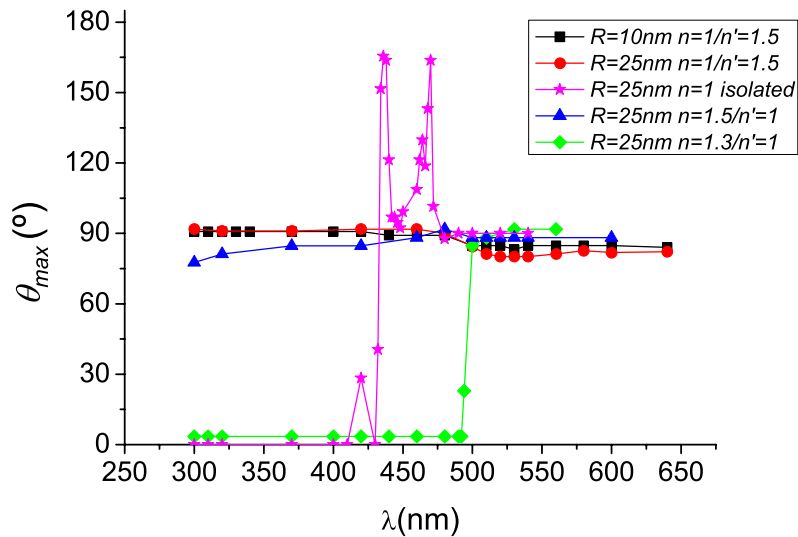


Fig. 11. Angular position of the maximum of the local electric field ( $\theta_{max}$ ) around a gold cylinder of two different sizes above a flat substrate, at a distance  $d=1nm$ , as a function of the incident wavelength and for different combinations of the refractive index of the surrounding medium and the substrate.

Below this wavelength, the maximum of the surface field is located in the gap between the particle and the substrate and tends to concentrate at both sides for longer wavelengths. Here, it is important to remark that, as happens for silver, the absolute value of the surface electric field reaches high values all around the cylinder for  $\lambda$  located around the transition zone ( $10^5$ - $10^6$  times the incident field). The sharp peaks observed in that region, with  $n>n'$  and when the cylinder is made of either silver or gold (Figs. 10 and 11 respectively), are due to the non-monotonic dependence of the refractive index of these materials [15] with the incident wavelength within the pseudo-matching interval. Therefore,  $\theta_{max}$  oscillates before reaching the dipolar behavior.

The different distributions within a transverse plane are illustrated in Fig. 12 for the case  $n=1.5$ ,  $n'=1$ , considering a gold cylinder of  $R=25nm$  and  $d=1nm$ , and for incident wavelengths well below, ( $\lambda=420nm$ ), well above ( $\lambda=560nm$ ) and inside the transition zone ( $\lambda=496nm$ ). In this figure, all the characteristics mentioned before can be observed. Similar plots are found for the transition associated to silver particle.

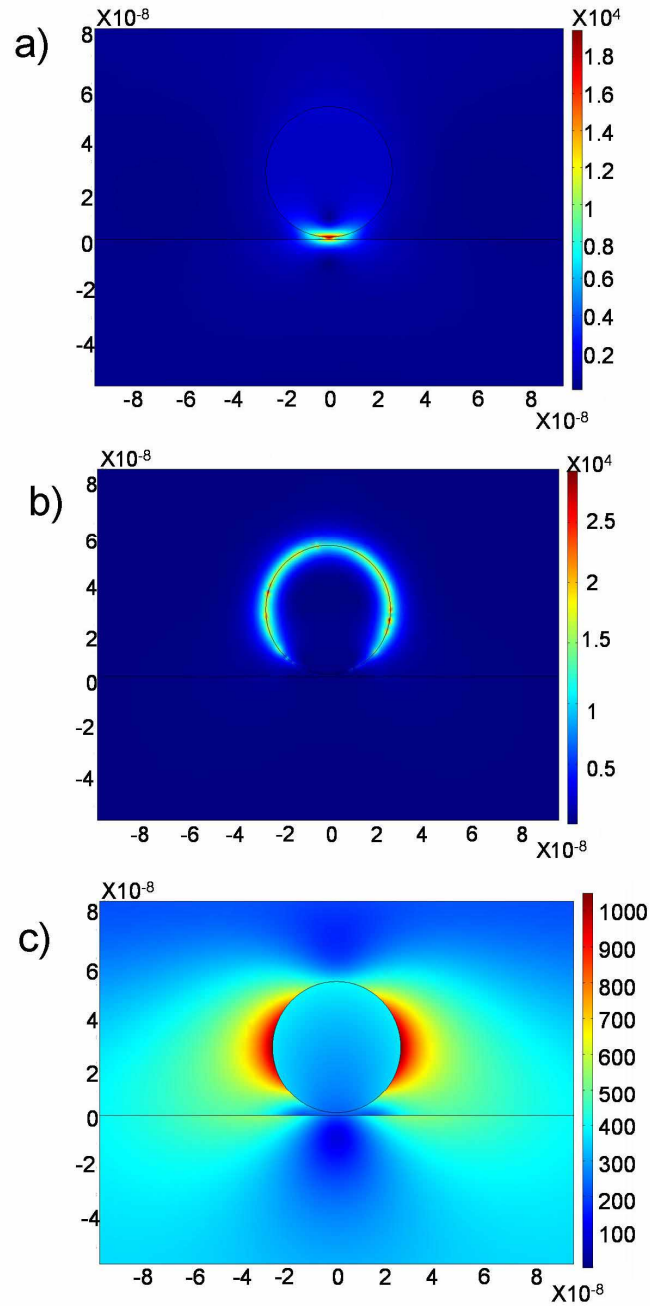


Fig. 12. Distribution of the electric field around a gold cylinder of radius  $R=25 \text{ nm}$  embedded in glass ( $n=1.5$ ) above vacuum at distance  $d=1 \text{ nm}$  for three different incident wavelength: (a)  $\lambda=420 \text{ nm}$ , (b)  $\lambda=496 \text{ nm}$  and (c)  $\lambda=560 \text{ nm}$

#### 4. Particle above a metallic substrate

This case has been widely studied before in the research carried out in [13]. The purpose of this section is to show some new features of this geometry when the particle is immersed in a

medium denser than vacuum. A typical experimental configuration is that of a metallic nanoparticle in water or other materials (pursuing a red shift of the resonance) and located at a certain distance above a metallic substrate [6, 8, 9]. In this situation the particle-substrate interaction is very strong, especially for small values of  $d$ , and the dipolar behaviour is completely lost. In fact, as it is outlined in ref [13], the maximum enhancement of the electric field is found in the space between the particle and the substrate and the charge distribution in the particle differs considerably from the typical “*eight*” shape. In the following, the chosen wavelengths are: 320 nm, 430 nm, and 600 nm, the first and the last located, respectively, below and above the transition zone (see Fig. 11), and the middle one,  $\lambda=430$  nm, corresponding to the pseudo-matching case, where  $|\text{Re } \epsilon_{Au}| \cong 1.69 = (1.3)^2$ . In Fig.13 (a), (b) and (c), the modulus of the electric field is represented for a gold particle,  $R=25$  nm, immersed in water ( $n=1.3$ ) and located above a metallic substrate of the same material (Au) at a distance  $d=1$ nm (very close to the substrate).

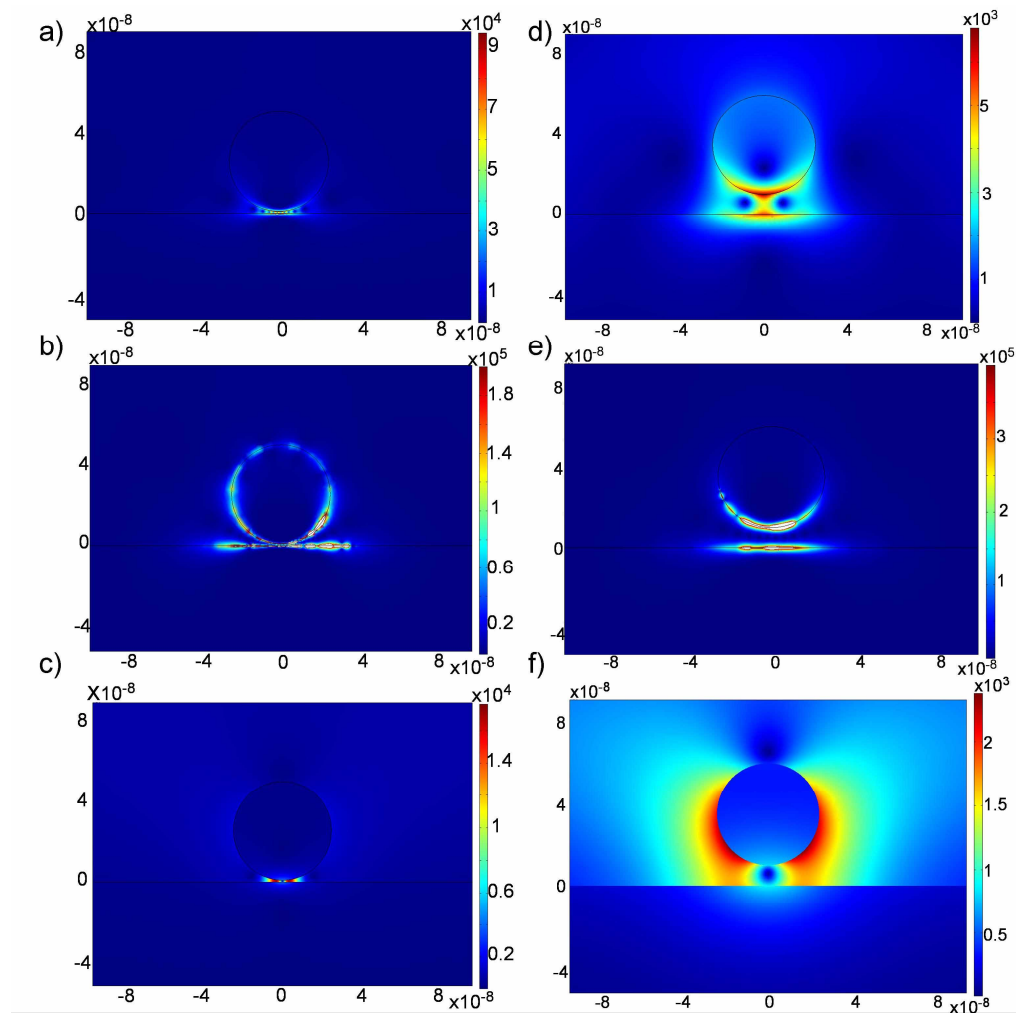


Fig. 13. Distribution of the electric field around a gold cylinder of radius  $R=25$  nm embedded in water ( $n=1.3$ ) above a gold substrate at distance  $d=1$ nm, (a) (b) and (c), or  $d=10$  nm, (d) (e) and (f), for three different incident wavelength: (a) and (d)  $\lambda=320$  nm, (b) and (e)  $\lambda=430$  nm and (c) and (f)  $\lambda=600$  nm.

Below and above the transition zone there is an important concentration of the electric field (values  $10^3$ -  $10^4$  times the incident field) in the gap between the particle and the

substrate. It is important to underline that for the transition zone ( $\lambda=430\text{ nm}$ ) the electric field is distributed all around the particle and can reach values as high as  $10^5\text{-}10^6$  near the gap. As the particle-substrate distance increases, the absolute value of the surface electric field on the particle decreases, as can be observed in Fig. 13 (d), (e) and (f) for  $d=10\text{ nm}$ . Below the transition zone (case  $\lambda\approx 320\text{ nm}$ ) there is still concentration of the electric field in the gap between the particle and the substrate but the distribution spreads out of the bottom part of the particle and its maximum values decreases. At  $\lambda=430\text{ nm}$ , very high values of the electric field can be found on the particle surface and the field distribution on the particle is more localized at the bottom part of the particle, on the contrary to what happens at closer separations where the surface electric field on the particle tends to be more uniformly distributed. Above the transition zone ( $\lambda=600\text{ nm}$ ), the dipolar behaviour starts to appear but due to the interaction with the substrate a deformation of the “eight” shape can be seen (remember the plot marked with squares in Fig. 9).

## 5. Summary and conclusions

In this paper we have analyzed the interaction between metallic nanostructures and substrates focusing our work on how the electric field on the particle surface changes under this interaction. Among other aspects, we have analyzed the evolution of the typical “eight-shape” dependence of the surface field of an isolated nanoparticle when it approaches a substrate.

Firstly, we have shown that for isolated scatterers the physics involved in the 2D scattering problem is very similar to that of the 3D, being the results found for the location of the maximum of the surface field on a cylinder representative of those found for a sphere.

Observing the spatial distribution of the electric field around the surface of an isolated sphere or an isolated infinite cylinder, we note how the angular position of the maximum of the local electric field ( $\theta_{max}$ ) evolves according to the system conditions. In particular, we showed that, as the particle size increases, or if the incident wavelength excites a localized plasmon resonance in the particle, the near field tends to deform the typical “eight-shape” of the dipolar behavior bending the maxima to the forward direction. This fact justifies the use of the parameter  $\theta_{max}$  to monitor the changes in the near field due to interactions with substrates.

When we consider an isolated silver cylinder in air we observe that for small values of the incident wavelength ( $\lambda < 320\text{ nm}$ ) the maximum of the local electric field appears in the backward direction ( $\theta=180^\circ$ ). This behavior changes when the modulus of the real part of the dielectric constant of the cylinder matches that of the surrounding medium. At this point the angular position of the maximum of the electric field flips to  $\theta=0^\circ$  and keeps on there for a certain range of  $\lambda$ . The wavelength at which this occurs depends on the size of the cylinder and the refractive index of the surrounding medium. Similar behavior appears for an isolated silver sphere. When we consider a gold cylinder or a gold sphere, the behavior is simpler because the maximum of the modulus of the surface electric field appears very close to  $90^\circ$  (dipolar behavior) in the whole range of wavelengths that we have studied due to the characteristics of the refractive index of gold.

The distribution of the surface electric field changes when a dielectric substrate is placed under the cylinder. As the particle approaches the substrate, the electric field localizes in the gap in a more stable way (the maximum of the local electric field tends to  $0^\circ$  for a longer range of wavelengths) and the dipolar behavior only appears for very long wavelengths. The origin of this strong concentration of the electric field in the gap between the particle and the substrate can be explained if we observe the evolution of the angular distribution of the local electric field as the gap distance changes: when the particle is far from the substrate, the typical “eight-shape” of the dipolar behavior is observed, with two maxima at  $\theta=90^\circ$  and  $\theta=270^\circ$ . As the particle approaches the substrate these two maxima shift to the forward direction and when the substrate is very close, those maxima are in the gap between the particle and the substrate. If the cylinder is immersed in a medium denser than the substrate, the electric field acquires the dipolar behavior ( $\theta_{max}=90^\circ$ ) at lower wavelengths than in the previous case.

Finally, we have studied a configuration that resembles others of typical experimental setups: a metallic particle (gold cylinder here) immersed in a medium denser than the vacuum (water in our case) and located above a metallic substrate (gold flat surface in our calculations). In this case, the interaction with the substrate is stronger, producing a concentration of energy in the particle-substrate gap, even below the transition wavelength (the point where the modulus of the refractive index of the cylinder matches that of the surrounding medium). Near this pseudo-matching wavelength the electromagnetic field acquires high values, and its surface distribution is quite uniform around the particle for small gap distances. As the gap distance increases, the localization and the maximum values of the electric field decrease, as expected. Above the matching wavelength the electric field tends to the dipolar shape.

### **Acknowledgments**

This research has been supported by the Ministry of Education of Spain under the project FIS2007-60158. Braulio García-Cámara thanks to University of Cantabria for his Ph.D. grant.